Topics in Catalysis
https://doi.org/10.1007/s11244-025-02063-6

ORIGINAL PAPER

Efficient Photodegradation of Methylene Blue Dye Using Biogenic Copper Doped Zinc Oxide (Cu@ZnO) Photocatalyst Under Ultra-visible Light Irradiation

Vikram Jadhav[1] · Umesh Dheple[1] · Pradnya Raut[2] · Seema Nikam[2] · Arun Bhagare[1]

Accepted: 16 January 2025

Abstract

The release of vast effluents in textile dyeing processes into water reservoirs is one of the critical environmental issues. The more toxic methylene blue (MB) dye used in textile industries is being utilized in a biogenic approach using the hydrothermal method to synthesize the Cu@ZnO nanomaterials through sustainable and environment-friendly process utilization of *Hibiscus rosa-sinensis* leaf extracts as reducing as well as capping agents. Several analytical techniques were used for the structural, morphological, and compositional attributes of the Cu@ZnO nanomaterials characterized by XRD, UV, FTIR, FE-SEM–EDS, and HR-TEM-SEAD analysis. The UV–Vis spectrum showed a peak absorbance at 380 nm and a band gap of 3.26 eV. FTIR analysis revealed several vibrational modes, indicating the presence of various functional groups such as 2355 cm^{-1} (C=O stretching), 1529 cm^{-1} (C=C stretching), 665 cm^{-1} (Cu–O stretching), and 426 cm^{-1} (Zn–O stretching). XRD analysis confirmed the crystalline nature of the nanomaterials with an average crystallite size of 32 nm. EDX confirmed the Cu, Zn, and O elements, and SEM and HR-TEM analyses revealed a sphere-like morphology with an interplanar spacing of 260 pm. The photocatalytic activity concerning MB dye degradation under ultraviolet–visible light exposure was determined. Effects of parameters, including catalyst dosage, initial dye concentration, and irradiation time, concerning the degradation efficiency. A degradation rate of 97.67% for MB dye was obtained within an irradiation time of 60 min with a remarkable photocatalytic efficacy of the nanomaterials. The kinetic analysis described the first-order reaction model by a determined velocity constant of 0.03390 min^{-1} and a half-life of 20.44 min. This can be attributed to its specific structural properties, which enhance the effective separation and transfer of charges in the nanomaterials. The current work is a promising basis for further developing sustainable and efficient photocatalysts to remedy water pollution from organic dye contaminants.

✉ Vikram Jadhav
mevikramjadhav@gmail.com

✉ Pradnya Raut
pradnyar_ioe@bkc.met.edu

[1] Department of Chemistry, M.V.P. Samaj's K. K. Wagh Arts, Science, and Commerce College, Pimpalgaon (B.), Nashik, Maharashtra 422209, India

[2] MET's Institute of Engineering, Bhujbal Knowledge City, Adgaon, Nashik, Maharashtra 422207, India

Published online: 13 February 2025

Graphical Abstract

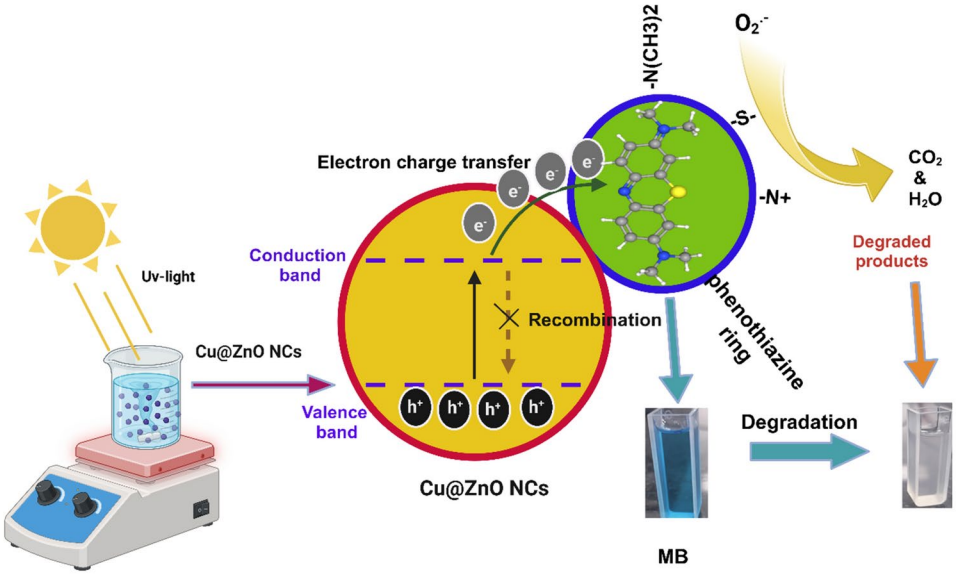

Keywords *Hibiscus rosa-sinensis* · Photocatalysis · Methylene blue · Cu@ZnO · Water pollution

Abbreviations

Cu@ZnO	Copper-doped zinc oxide
MB	Methylene blue
UV–Vis	Ultra violet-visible
FTIR	Fourier transform infrared spectroscopy
XRD	X-ray diffraction
FE-SEM	Field emission scanning electron microscopy
EDX	Energy dispersive X-ray spectroscopy
TEM	Transmission electron microscopy
SARD	Selected area electron diffraction
A.R	Analytical reagent
JCPDS	Joint committee on powder diffraction standards
VB	Valence band
CB	Conduction band

1 Introduction

Water pollution, one of the most serious global issues, has gained attention through industrialisation and urbanisation. The textile industry emits large amounts of organic dyes into aquatic ecosystems, which results in tremendous environmental and health hazards [1–3]. Methylene Blue (MB) is a hazardous cationic dye owing to its toxic, carcinogenic, and persistent characteristics. Conventional wastewater treatment strategies often struggle with such contaminants, meaning it is of utmost importance to promote research to develop innovative and sustainable technologies [4–6]. In recent years, photocatalysis technology has emerged with more potential and prominence as a creative technique for degrading organic pollutants. Illuminating the photocatalysts based on semiconductors generates highly reactive species, including $^{\bullet}OH$ and $^{\bullet}O_2$, which have a high potential to oxidise and mineralise organic pollutants. [7]. Among different kinds of semiconductor photocatalysts, researchers have studied ZnO because of its non-toxicity, biological compatibility, photocatalytic activity, and drug-delivery system [8–10]. Even though the band gap for ZnO is vast, visible light is not sufficiently absorbed and becomes pretty weak in photoactivity. To overcome the limitation above, metal doping has been done by modifying the electronic configuration of ZnO and widening the spectrum of light absorption [11, 12]. Copper (Cu) doping can produce promising outcomes for improved photocatalytic performance in ZnO. This involves incorporating copper ions into the ZnO lattice and results in localised energy states within the bandgap, allowing for better visible light absorption and enhanced efficient charge separation [13, 14]. Nanomaterials' application for remediating dyes in wastewater is a rapidly growing domain because of the need to minimise industrial dyes' environmental and health risks. Compared to traditional methodologies, nanomaterials have a vast surface area, enhanced reactivity, and superior performance in ecological remediation. For instance, the photocatalytic characteristics of ZnO nanocomposites have been proven to efficiently decompose cationic and anionic dyes, such as MB and Congo Red. ZnO hexagonal wurtzite crystalline

configuration enhances its photocatalytic efficacy, and it is an up-and-coming candidate for sustainable dye degradation methods [15, 16]. SnO_2 nanoparticles doped with lanthanum have shown catalytic performance with degradation rates up to 94% for Rhodamine B under UV irradiation with structural maintenance of the medium cycle number. We also investigated the incorporation of Cu into TiO_2 composites. We provided empirical evidence that these composites can achieve an efficiency of up to 99.12% for acid green dye, highlighting metal-doped nanomaterials' capacity to improve dye removal efficiency. Additionally highlighted are the functions of nanoparticles as catalysts in sophisticated oxidation processes that, under ideal operating conditions, can remove organic contaminants up to 99 per cent and special bioenergetic processes like membranes and pH gradient-based particles that occasionally work inside or on particles to separate communities from toxic environments. Nanomaterials can demonstrate their adaptability in dye removal but also possess the ability to remediate air pollution and store energy, demonstrating their multifunctional potential [17]. These represent a prominent advancement in solving the inherent complexities of pollution and ongoing investigations of the refinement of their properties and extension of their applications [18–21].

More recent efforts are being made to develop green and sustainable synthesis methodology for nanomaterials. Biogenic synthesis uses plant extracts as reductive and capping agents, which has many merits compared to the traditional chemical route, such as an inexpensive process, environmental acceptability, and the opportunity to generate nanomaterials with customised size and morphology [22, 23]. The hibiscus rosa-sinensis plant (Fig. 1) is commonly called the Chinese hibiscus. This flowering plant species is native to East Asia and has been selectively bred for its colourful flowers for thousands of years. Besides being an ornament, this plant has been studied for other practical applications in ethnobotany and environmental cleanup [24].

Fig. 1 *Hibiscus rosa sinensis* leaves

In recent studies, *Hibiscus rosa-sinensis* has shown utmost interest to the academic fraternity as a biologically obtained reducing, stabilising, and capping agent for synthesising metal and metal oxide nanomaterials. Plant extracts are rich in phytochemical compounds like polyphenols, flavonoids, and terpenoids, with exceptional reducing and stabilising abilities [25]. These biological agents can chelate with metal ions, reducing them to nanoparticles while also stopping them from clumping together. Using plant extracts for biogenic synthesis of materials has several advantages over the traditional chemical process, including cost-effectiveness, environmental sustainability, and ease of creating nanoparticles with the appropriate size and shape [26]. The reducing and capping abilities of *Hibiscus rosa-sinensis* leaf extract efficiently synthesised Cu@ZnO nanomaterial with promising photocatalytic potential for the degradation of organic pollutants [22].

In this work, Cu@ZnO nanomaterial was synthesised biogenically through the *Hibiscus rosa-sinensis* leaf extract. The synthesised nanomaterial was characterised through several characterisation techniques, such as XRD, UV–Vis, FTIR, SEM–EDX, and HR-TEM-SEAD analysis, to probe its structural, morphological, and compositional features. The photocatalytic efficiency of the as-synthesized nanomaterial was checked for the degradation of MB dye under UV–Vis light irradiation. Degradation efficiency was checked for parameters, namely catalyst dosage and irradiation duration. Kinetics of degradation and the mechanisms were studied to understand the photocatalytic process. This research aims to produce sustainable photocatalysts for the breakdown of organic dyes in water. Combining metal doping and biogenic synthesis advantages, we synthesized a highly active Cu@ZnO nanomaterial with exceptional photocatalytic performance under UV–visible light irradiation. The current study provides a promising framework for producing safe and profitable water filtration systems.

2 Materials and Methods

2.1 Materials

Metal precursors copper nitrate ($Cu(NO_3)_2.3H_2O$) and zinc nitrate ($Zn(NO_3)_2.\ 6H_2O$) were purchased from

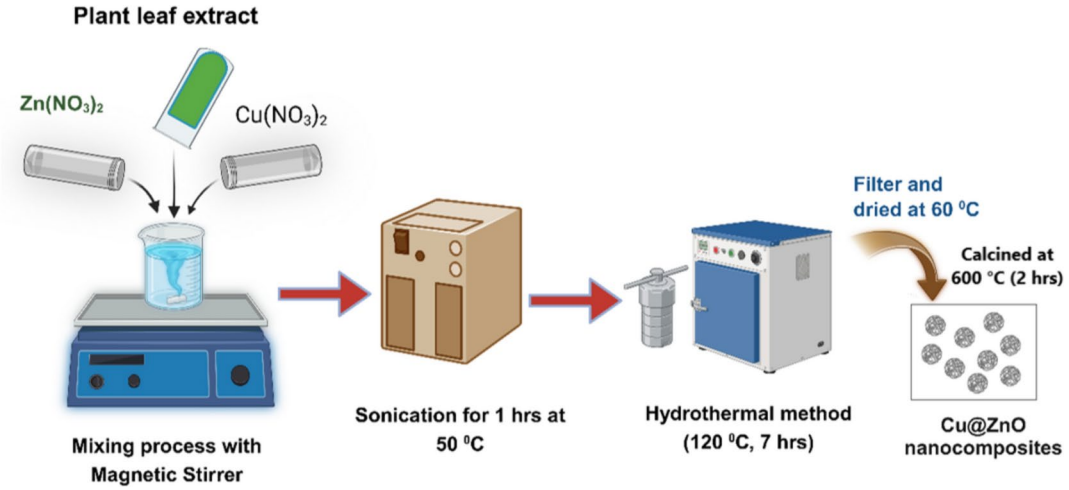

Fig. 2 Experimental method for the synthesis of Cu@ZnO nanomaterial

Sigma-Aldrich. Organic Dye MB was bought from Loba Chemie. All chemicals used during the experiment were of A.R. grade. They were used directly, without further purification. Deionised water of Chargo Chemicals and Fresh Leaves of *Hibiscus rosa-sinensis* collected from a local agricultural field in Pimpalgaon (B), Nashik**.**

2.2 Methods

2.2.1 Synthesis of Plant-Mediated Cu@ZnO Nanomaterials

The leaves of *Hibiscus rosa-sinensis* were collected, dried, and then ground into powder. The powdered material was extracted using deionised water in combination with a Soxhlet extractor to obtain the plant leaf extract. $Cu(NO_3)_2.3H_2O$ was dissolved stoichiometrically in deionised water, to which the leaf extract was added. An equivalent stoichiometric quantity of $Zn(NO_3)_2.6H_2O$ was added to the sonicated solution (1 h; 50 °C) and stirred vigorously to maintain a pH value of approximately 10, adjusting it with sodium hydroxide solution. This obtained solution was added into the autoclave, where the hydrothermal treatment was conducted at 120 °C for seven hours. After the hydrothermal treatment, the precipitate was filtered, washed, dried in the oven, and calcined (Fig. 2), and the obtained nanomaterial was analysed using several methods.

Photocatalytic Activity of MB Dye Degradation: A synthesised Cu@ZnO nanomaterial was subjected to photocatalytic activity studies using the model pollutant MB dye. For MB concentration, a steady concentration at 10^{-5} M is used, and the concentration levels of the nanomaterial were prepared systematically at 10 mg/100 mL concentration. To evaluate any degradation that occurs due to the adsorption of the reaction mixture containing MB and nanomaterial, the latter was left in the dark for 10 min. The reaction

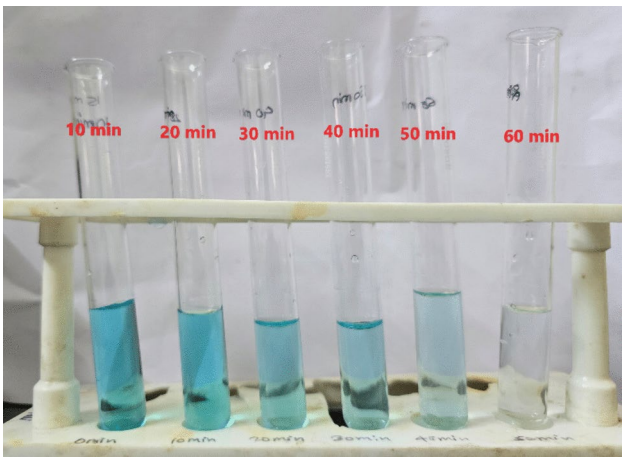

Fig. 3 MB dye solution at different time (min) interval

mixture was then subjected to a maximum irradiation period of 60 min using UV–Vis light. The kinetics of MB degradation were monitored by analysing the absorbance spectra of the reaction mixture at specified time intervals, and we found the change in the colour of the solution (Fig. 3). The decrease in the dye's concentration can be monitored through a decline in peak intensity centred at the characteristic wavelength of 664 nm. MB revealed very slight degradation in the absence of light, proving that the primary degradation mechanism is photocatalytic.

However, when UV–Vis light was applied, there was a significant decline in absorbance of the MB peak over time, which showed degradation of the dye. The degradation of MB happened at a faster rate because of the increased concentration of Cu@ZnO nanomaterial, which a quicker decrease in absorbance could have proved. By using the following formula (Eq. 1) for measurement of the % degradation of MB dye;

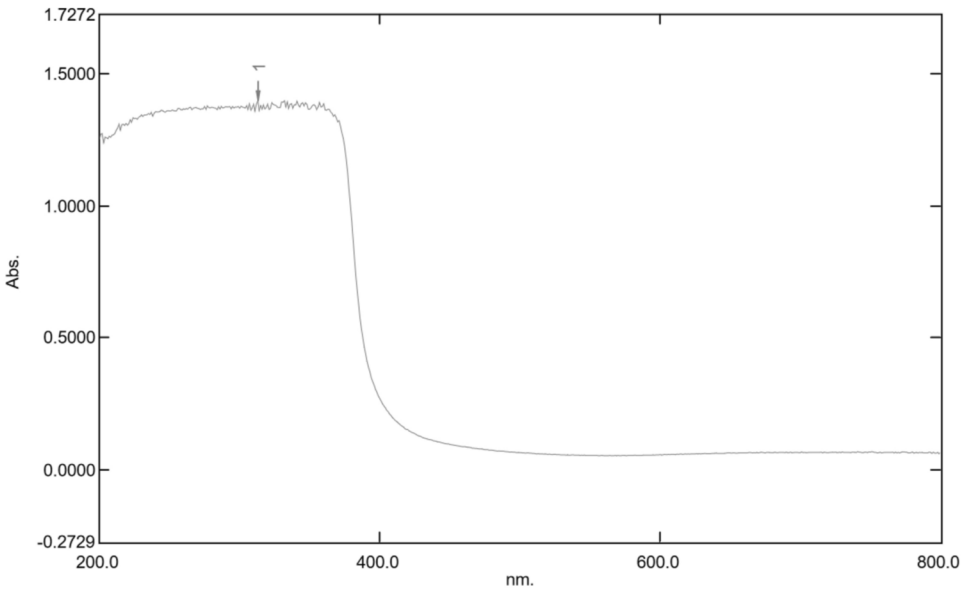

Fig. 4 UV–Vis spectra of Cu@ZnO nanomaterial

$$\% \text{ of MB dye degradation } = \frac{[A]_0 - [A]}{[A]_0} \times 100 \quad (1)$$

where $[A]_0$ and [A] are the Initial absorbance (t=0 min) and Absorbance (t=t min) of the MB dye solution. Calculation of the data gives the maximum amount of the degradation of MB as high as 97.67% at 10 mg/100 mL with Cu@ZnO nanomaterial at 60 min. The interaction between Cu and ZnO enhances photocatalytic efficiency, as it effectively facilitates charge separation and generates radicals. [27, 28].

3 Results and Discussion

3.1 UV–Vis Analysis

The UV–Vis absorption spectrum of the Cu@ZnO nanomaterial exhibited a significant absorption band in the ultraviolet region, with the maximum absorption wavelength (λmax) measured at 380 nm (Fig. 4). This absorption band is due to ZnO's characteristic intrinsic bandgap absorption feature.

The Eg value of the Cu@ZnO nanomaterial was obtained for the band gap using the following Eq. (2) [29, 30]:

$$\begin{aligned} \text{Eg } &= 1240 / \lambda\text{max}, \ (\lambda\text{max } = 380 \text{ nm}) \\ &= 1240 / 380 \\ &= 3.26 \text{ eV} \end{aligned} \quad (2)$$

This means that the material may very well absorb UV light, consistent with the absorption spectrum, where a sharp absorption peak in the ultraviolet region is observed. This is because a relatively high band gap energy would involve the highly energetic generation of electron–hole charge carrier pairs when subjected to photoexcitation; this, in paradoxical interaction, degrades the organic pollutants through catalysis [31].

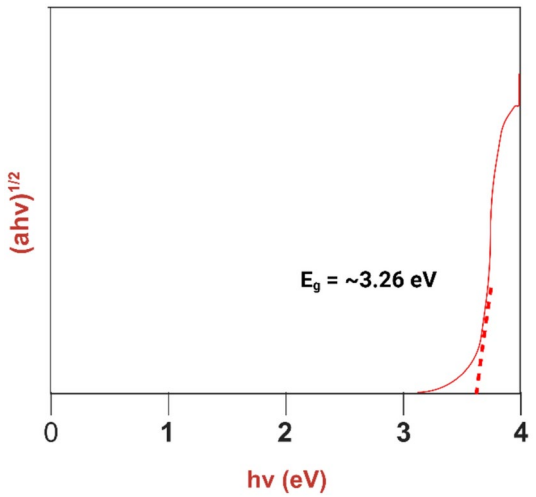

Fig. 5 Tauc plot of Cu@ZnO nanomaterials

The Tauc plot is a graphical presentation used to determine the bandgap of semiconductors from their optical absorption spectra. For nanomaterials, the direct bandgap, which ranges to 3.26 eV (Fig. 5), was found in the plot. Therefore, Tauc plots have become a reliable way to calculate this parameter to design and optimise semiconductor devices. Cu incorporation may lead to impurity levels within the band gap of ZnO, thereby modifying the band gap energy and enhancing the absorption of visible light. Cu doping may also improve charge separation efficiency because it can act as an electron trap, thus preventing the recombination of the photogenerated charge carriers [32, 33].

3.2 FTIR Analysis

The FTIR analysis of the green synthesised Cu@ZnO nanomaterials is given in the following Fig. 6.

It reveals characteristic absorption peaks at 3744, 2969, 2355, 1529, 1384, 1074, 665, and 426 cm^{-1}, which indicate the following functional groups [7, 23, 34]: 3744 cm^{-1}: O–H stretching associated with hydroxyl moieties. 2969 cm^{-1}: C–H stretching characteristic of aliphatic hydrocarbons, 2355 cm^{-1}: O=C=O stretching attributed to carbon dioxide. 1529 cm^{-1}: C=C stretching linked to aromatic structures. 1384 cm^{-1}: C–H bending corresponding to methyl groups. 1074 cm^{-1}: C–O stretching related to alcohols or ethers. 665 cm^{-1}: Cu–O stretching indicative of CuO presence. 426 cm^{-1}: Zn–O stretching representing ZnO presence. Identifying these functional groups corroborates the successful fabrication of the Cu@ZnO nanomaterials. The O–H stretching peak observed at 3744 cm^{-1} signifies the existence of hydroxyl groups on the nanomaterial surface, which may play a pivotal role in its photocatalytic efficacy. The C–H stretching peak at 2969 cm^{-1} implies the presence of organic contaminants originating from the plant leaf extract utilised during the synthesis process. The C=O stretching peak at 2355 cm^{-1} could potentially arise from oxidized organic substances. The C=C stretching peak at 1529 cm^{-1} is plausibly linked to aromatic compounds derived from the plant leaf extract. The Cu–O stretching peak at 665 cm^{-1} and the Zn–O stretching peak at 426 cm^{-1} substantiate the incorporation of CuO and ZnO within the nanomaterial's matrix. [12, 35].

3.3 XRD Analysis

Figure 7 shows the detected XRD pattern for Cu@ZnO nanomaterial.

The peaks' intensity and position give the nanomaterial's structure, phase, and crystallite sizes. In the diffractogram, peaks at 31.768°, 34.420°, 36.254°, 47.539°, 56.601°, 62.867°, 66.383°, 67.960°, 69.088°, 72.553°, and 76.976° correspond to the (100), (002), (101), (102), (110), (103), (200), (112), (201), (004), and (202) planes, these peak positions are in excellent agreement with the standard JCPDS card No. 89-7102 for Cu@ZnO nanomaterial [28, 31, 36]. For the Cu@ZnO nanomaterial, a crystallite size of about 32 nm was obtained using Scherrer's formula.

3.4 FE-SEM Analysis

The FE-SEM images clearly show that the Cu@ZnO nanomaterial has a complex hierarchical structure. The nano-sized particles are well dispersed in the larger aggregates, thus contributing to their unique physical properties. This morphology, combined with an average particle size of about 75 nm (Fig. 8), significantly increases the available

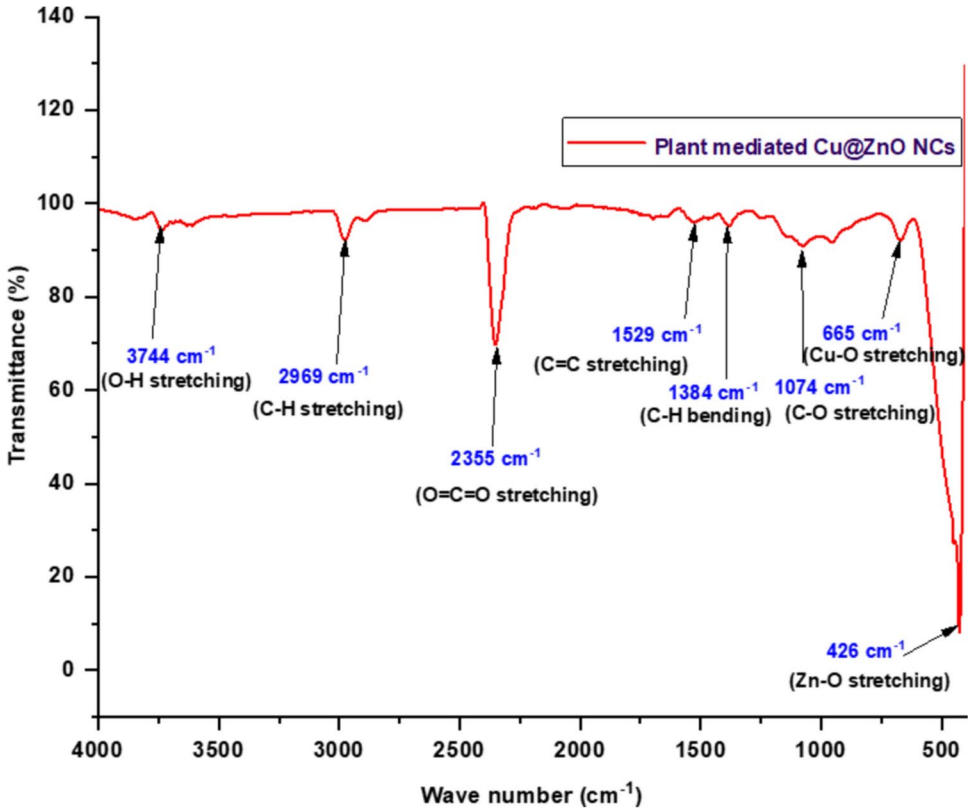

Fig. 6 FTIR spectra of Cu@ZnO nanomaterials

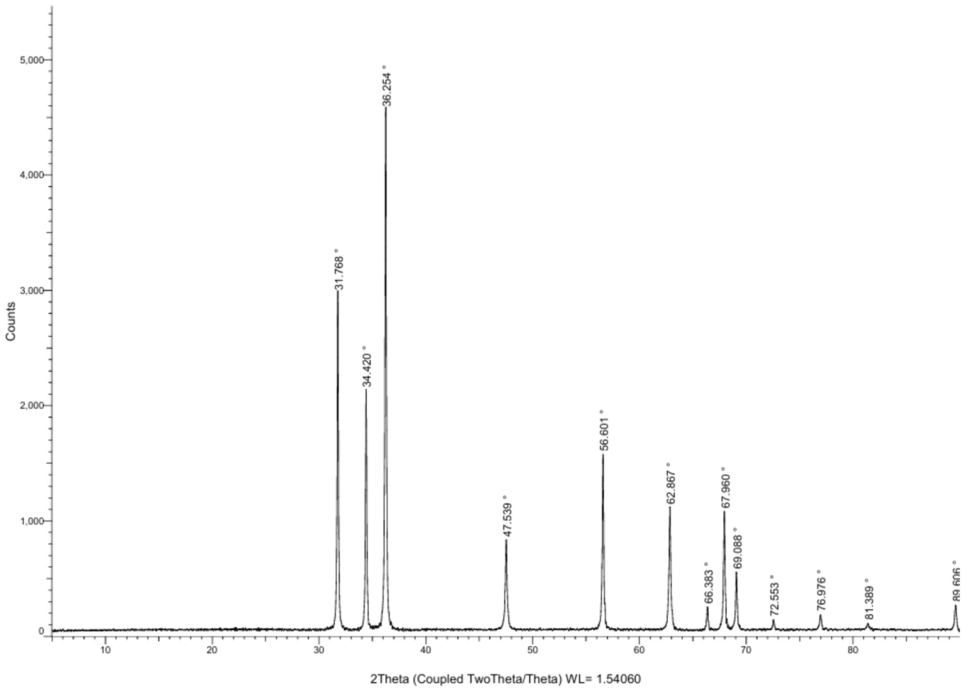

Fig. 7 XRD spectra of Cu@ZnO nanomaterials

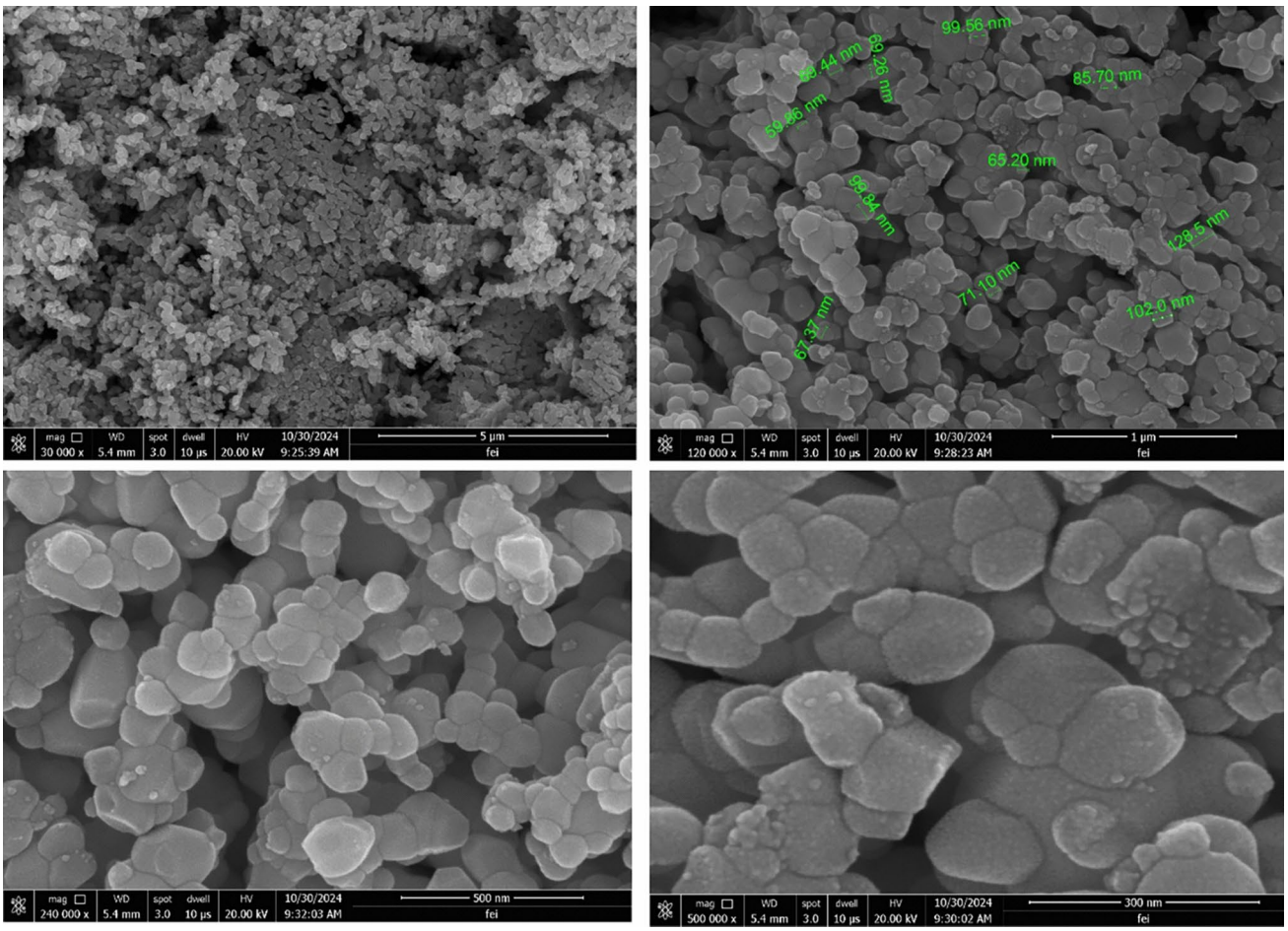

Fig. 8 FE-SEM analysis of Cu@ZnO nanomaterial

surface area, which enhances better absorption of light and interaction with dye molecules in the environment [37] [38].

Combining these factors with the structural hierarchy, as outlined above, allows one to understand how the two work synergistically together to enhance photocatalytic activity with an efficiently effective degradation product of MB dye upon ultra-visible light irradiation [6].

3.5 EDX Analysis

The EDX analysis of the synthesized Cu@ZnO photocatalyst has also clearly established the presence of anticipated constituent elements in the compound, such as copper (Cu), zinc (Zn), and oxygen (O) (Fig. 9). As a result, the available evidence on the composition of the catalyst that is prepared is considerable. The following is used for each of the atomic percentages concerning each element. The evident existence of Cu and Zn in the structure is sufficient as a high confirmation that Cu has doped well into the framework of the ZnO lattice as a significant step toward photo-catalytic properties enhancement of the material oxygen (O): 59.89% Cu: 17.08% Zn: 23.03%.

The very remarkable oxygen concentration in the analysis indicates high abundance and points toward the presence of oxygen vacancies, which are essential features that can act as active sites for photocatalytic reactions. EDX analysis further confirms the formation of the Cu@ZnO nanomaterial, which is a necessary factor in enhancing the photocatalytic activity of the material. Cu dopants in ZnO are instrumental in developing defects and creating new energy levels within the gap. This has a remarkable enhancing effect on the ability of charge separation while minimizing the recombination of photogenerated electron–hole pairs. This may lead to a higher amount of charge carriers that will readily be available to influence redox reactions, thus making for effective degradation of the dye [28, 31].

3.6 TEM-SEAD and Line Profile Analysis

With close observation, the TEM images indicate the spherical morphology of Cu@ZnO nanomaterial, confirming the necessity of the particular geometrical configuration and the form presented. Due to a spherical shape that can extensively exhibit high surface area facilitating absorption properties for light intensity, which enhances the photocatalysis material with molecular dyes interaction, their efficiency is highly promising for such performance. It is found that the interplanar spacing observed in the TEM images is about 126 pm, a measured value directly related to the (101) crystallographic plane of ZnO (Fig. 10). Such an interplanar spacing gives well-defined crystalline structures in the nanomaterials and its implication for the photocatalytic phenomena. Through TEM analysis, it has been well established that both spherical morphology and crystalline

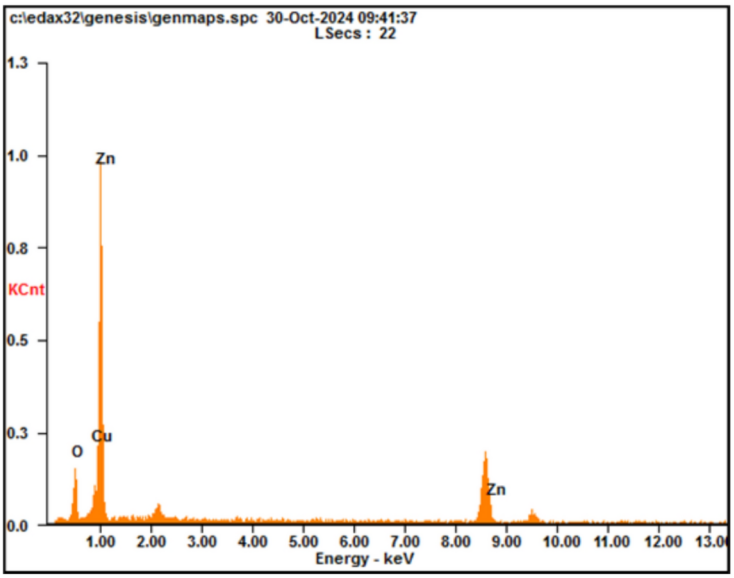

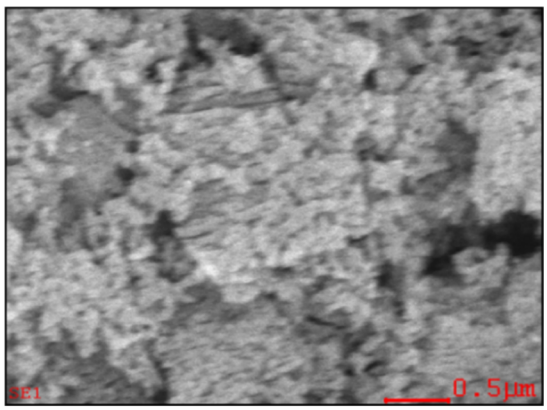

Element	Wt%	At%
OK	27.00	59.89
CuL	30.59	17.08
ZnK	42.42	23.03
Matrix	Correction	ZAF

Fig. 9 EDX analysis of Cu@ZnO nanomaterial

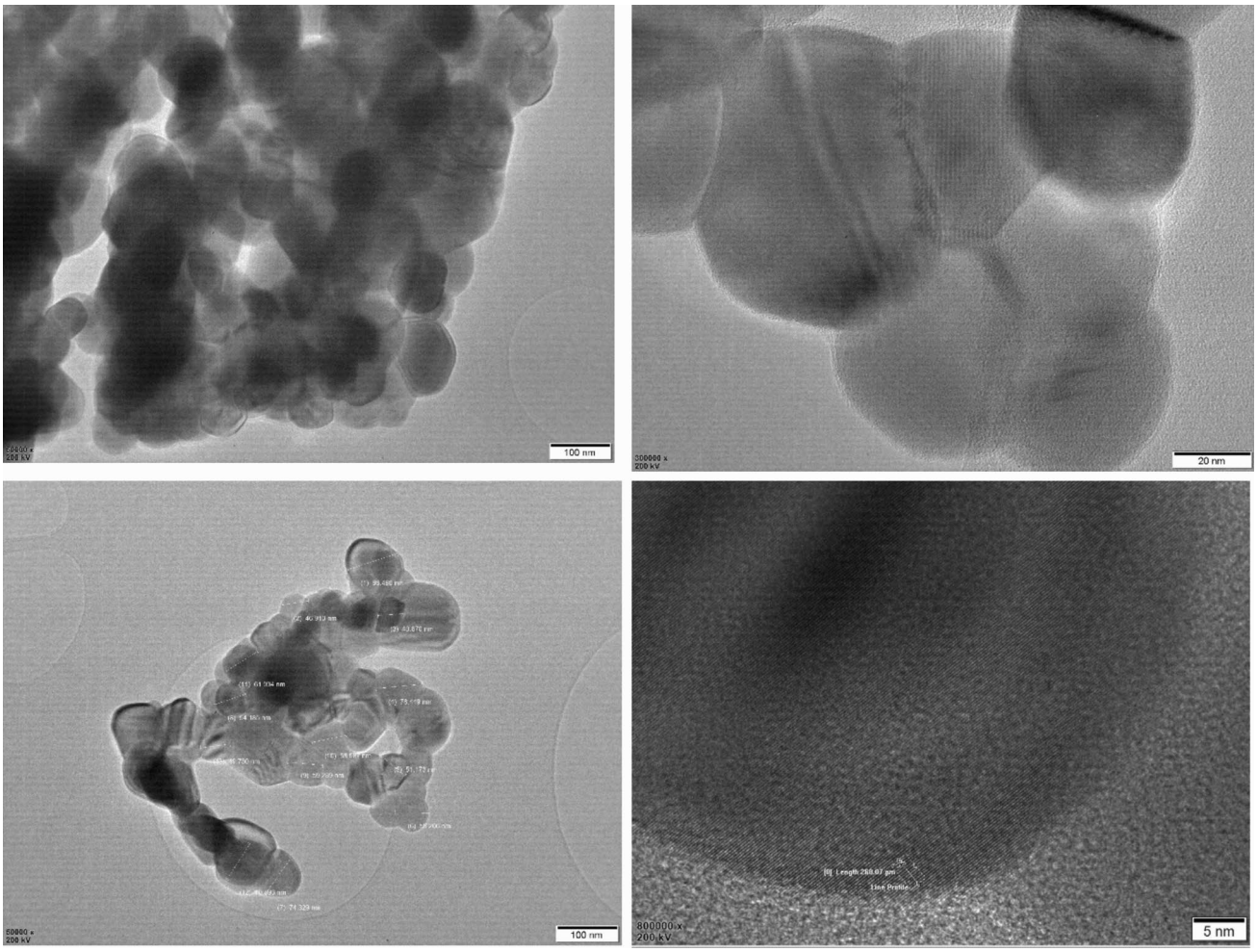

Fig. 10 TEM analysis of Cu@ZnO nanomaterial

features are decisive features of the Cu@ZnO photocatalyst and contribute to its efficacy in photocatalytic applications [32, 36, 39].

The spherical morphology accompanied by the well-defined crystalline structure of the Cu@ZnO nanomaterial is closely associated with a higher photocatalytic activity, which gives a better understanding of the functional capabilities of such material. The above spherical morphology is beneficial because it offers a significantly large surface area, enhancing active sites' availability for effective light absorption and interaction with dye molecules [40, 41]. Such an enhancement results in a notable improvement in light harvesting efficiency, thereby contributing to an overall enhancement in photocatalytic performance. Another aspect related to the nature of nanosized crystals is the promotion of effective charge separation. Charge carriers formed on the occasion of photon incidence may, due to the migration to the nanoparticle's surface, either be away from the sites of excitons, or their recombination might be significantly hindered. This movement is crucial in that sense, as it allows such charge carriers to seek redox reactions to prevent them from recombining again and thus enhancing photocatalytic performance [33, 42].

The SEAD pattern displays clear concentric rings, a prominent feature evident in the gathered data. This validates the polycrystalline nature of the Cu@ZnO photocatalyst, indicating its composition of multiple crystalline grains (Fig. 11). The presence of several visible rings in the SEAD patterns significantly indicates the existence of different crystallographic planes within the material, which corresponds to the hierarchical structure previously established through detailed investigations [43, 44].

Line profile analysis is among the essential techniques to determine the material's structural features at the nanoscale. This technique is very valuable information regarding the interplanar spacing within the nanomaterial, which considerably determines the material's properties. The distinct peaks in the line profile directly relate to specific crystallographic planes that allow for precise identification of the material's structural characteristics (Fig. 12). From the

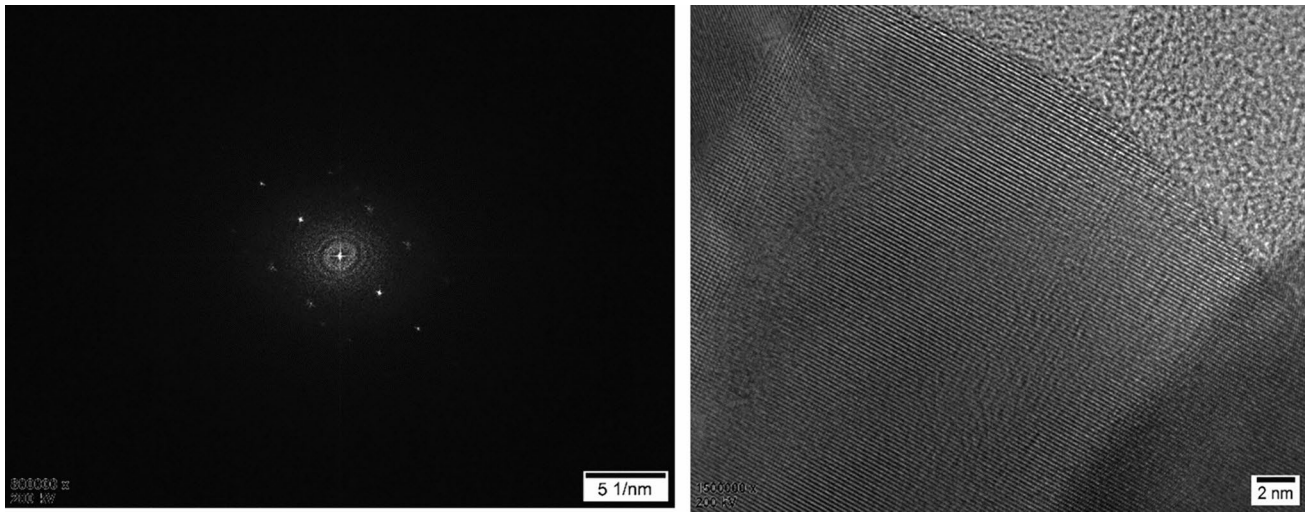

Fig. 11 SEAD pattern of Cu@ZnO nanomaterial

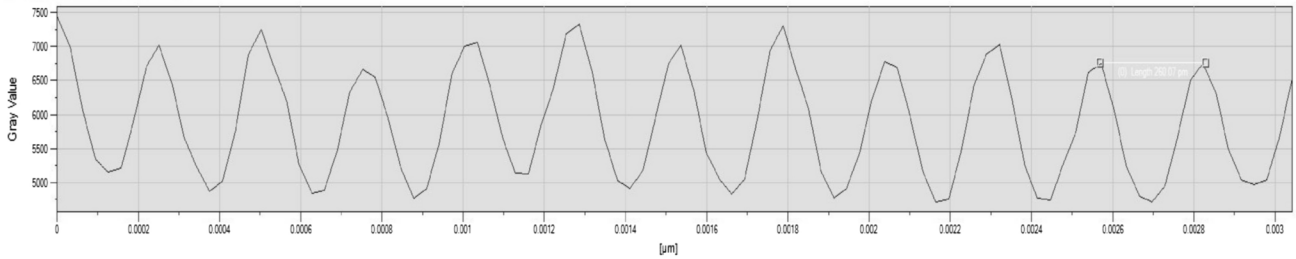

Fig. 12 Line profile analysis of Cu@ZnO nanomaterials

above precise investigation of these peaks. It has become possible to determine the interplanar spacing correctly and then distinguish the different phases that exist within a sample from its crystallography, which explains the sample's overall behavior, conclusively confirming the polycrystalline nature of the Cu@ZnO photocatalyst by combined findings arising from both the SEAD and line profile analyses while providing valuable insight into intricate crystallographic structures essential to a better understanding of the photocatalytic properties exhibited by this material. This detailed information is not only crucial but also imperative for further exploration and application of the photocatalyst in various fields and, thus, enables advances in the field of material science and engineering [45–49].

4 Possible Mechanism of Photocatalytic MB Dye Degradation

The proposed mechanism of the photocatalytic degradation process for MB dye based on the utilization of Cu@ZnO nanomaterial when it is under irradiation by ultra-visible light may be illustrated by the following [22]:

Photoexcitation: The incident light energy (hv) has an energy value more than the inherent material's band gap (Eg). It excites the photocatalyst and, through photoexcitation, elevates the electrons e- from the VB (valence band) to CB (conduction band) and leaves the positive charge holes in VB that are h^+. *Charge separation and transfer:* The released electrons and holes then travel toward the surface of the Cu@ZnO-based photocatalyst (Eq. 3). Defect states are formed since the crystalline lattice structure of ZnO contains introduced dopant copper. Such a defect state can successfully trap the photogenerated charge carrier, thus further increasing the possibility of suppressing the recombination. Increased charge separation efficiency maximizes the photocatalytic material's overall photocatalytic activity.

Reduction: Generated electrons from the photocatalytic process react with O_2 adsorbing from the photocatalyst's surface, which evolves superoxide radicals (O_2-) (Eq. 4). Superoxide radicals are very oxidizing agents that can initiate the oxidation reaction of methylene blue dye molecules in the reaction solution. *Oxidation:* In the meantime, the holes that have been generated due to the photocatalytic activity react with the water molecules (H_2O) or hydroxyl ions (OH^-) to form hydroxyl radicals ($OH^•$) (Eq. 5). The hydroxyl radicals are very reactive and can be used to

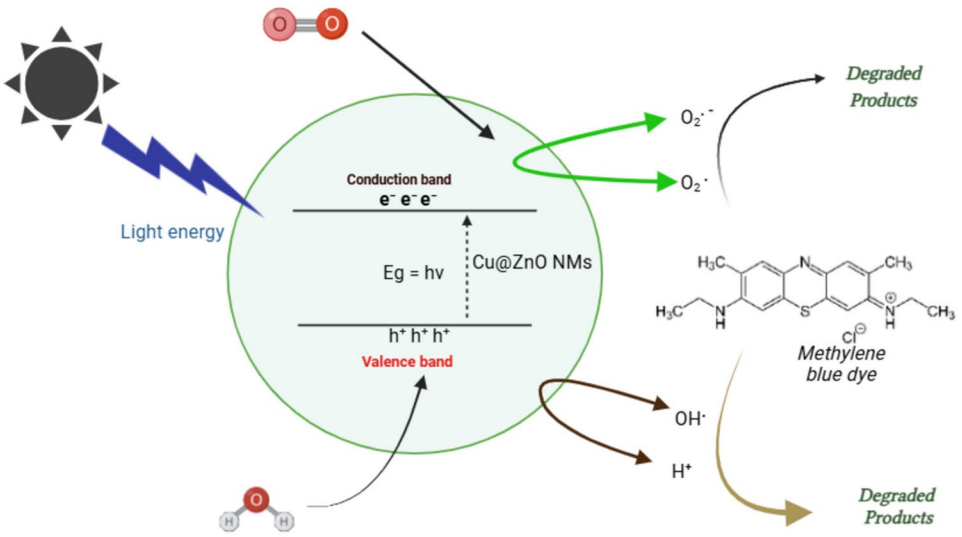

Fig. 13 Photocatalytic MB dye degradation using plant-mediated Cu@ZnO nanomaterials [22]

oxidize the methylene blue dye molecules successfully, which leads to their ultimate degradation into smaller and more nontoxic chemical species. *Dye Degradation:* The superoxide and hydroxyl radicals produced in the reactions above as aggressive oxidizing species broke the chemical bonds of dye molecules to degrade the dyes into fragments of their smaller sizes (Eq. 6).

The photochemical reactions can be written below:

$$\mathrm{Cu@ZnO} + \mathrm{hv} \rightarrow \mathrm{Cu@ZnO}\ \left(\mathrm{e}^- + \mathrm{h}^+\right) \quad (3)$$

$$\mathrm{O_2} + \mathrm{e}^- \rightarrow \mathrm{O_2^-} \quad (4)$$

$$\mathrm{H_2O} + \mathrm{h}^+ \rightarrow \mathrm{OH^{\cdot}} + \mathrm{H} \quad (5)$$

$$\mathrm{MB\ dye} + \mathrm{O_2} + \mathrm{OH^{\cdot}} \rightarrow \mathrm{Degraded\ products} \quad (6)$$

Introducing Cu dopants in the ZnO is essential as they cause defect states that trap charge carriers photogenerated quite efficiently, thus reducing their recombination and significantly enhancing the separation of charges. In such a system, incorporating these copper dopants might also act as an acceptor of electrons, thus enabling charge separation and increasing photocatalytic activity within the system. Due to a unique hierarchical structure and difference in the size of the particles, Cu@ZnO has an enlarged spectrum of light absorption range in which visible light takes part; hence, its photocatalytic application becomes fully able to utilize the energy from solar light. Effective Charge Separation: The hierarchical structure, along with the dopant copper, facilitates effective charge separation, which decreases the recombination of the photogenerated e^- and h^+ pairs and yields higher photocatalytic activity [2, 31, 39] (Fig. 13).

Photocatalytic degradation of MB dye by Cu@ZnO nanomaterial under ultra-visible light irradiation was followed by absorbance measurement of the MB solution at different time intervals (Table 1).

Table 1 Absorbance and rate constant of MB dye at different time intervals

Time (min)	Absorbance [A]	Log [A]	Rate constant (K) min^{-1}	Mean (K) min^{-1}
10	0.7169	−0.1445	2.655×10^{-2}	3.390×10^{-2}
20	0.6795	−0.1678	1.598×10^{-2}	
30	0.4052	−0.3923	2.789×10^{-2}	
40	0.2795	−0.5536	3.020×10^{-2}	
50	0.1265	−0.8979	4.002×10^{-2}	
60	0.02173	−1.8951	6.271×10^{-2}	

The degradation rate was assessed by determining the logarithm of absorbance (Log[A]). The K parameter is obtained using the rate constant value in the case of degradation reaction by observing the linear plot between the log[A] and the time. K is calculated by taking an average of rate constants to achieve the rate for the overall degradation. The dye solution's initial absorbance $[A]_0 = 0.9354$**.** Table 1 of obtained rate constants for the photocatalytic degradation of MB dye using the nanomaterial: Average rate constant $= 3.390 \times 10^{-2}\ min^{-1}$. The results show that the nanomaterial has excellent photocatalytic activity towards the degradation of MB dye. The decrease in absorbance with time is a confirmation of the degradation of the dye (Fig. 14). A higher rate constant points to the faster rate at which degradation occurs [36, 42, 50].

A relatively gradual rise in the dye's degradation is recorded (Table 2). In 20 min, it is roughly 23–27%. This induction phase may thus be connected with the initiation of photocatalyst's activation and the sequential formation of reactive species. The degradation rate sharply increases in the range of 20 to 40 min. Approximately 43% of the dye is degraded in this region. The increased degradation rate can be attributed to the increased concentration of reactive

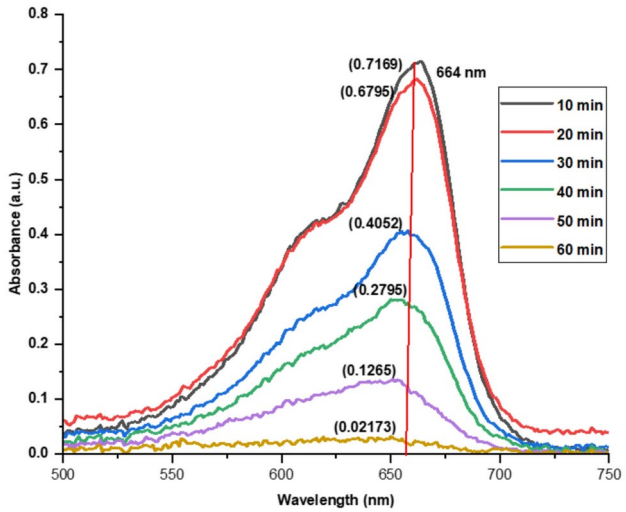

Fig. 14 Absorbance vs wavelength (nm) of MB dye degradation

Table 2 % of MB dye degradation using Cu@ZnO nanomaterials

Time (min)	% Dye degradation
10	23.35
20	27.36
30	56.68
40	70.12
50	86.48
60	97.67

species and efficient utilization of photoenergy. The degradation rate slows in the last 20 min, but the remaining dye is almost completely degraded. This reaches a degradation percentage of 97.67% at 60 min (Fig. 15).

$$t_{1/2} = \frac{0.693}{0.03390} = 20.44 \text{ min} \quad (7)$$

This 20.44 min $t_{1/2}$ of degradation for the MB dye thus signifies a half-effective degradative mechanism (Eq. 7). The same parameter states that the given system can decrease the dye concentration up to fifty percent within that period. Diminished $t_{1/2}$ would, thus, correspond to the accelerated degradation rate, which will signify the more efficacious catalytic systems.

This result shows that the photocatalytic process effectively removes the dye from the aqueous solution. In General, the Cu@ZnO nanomaterial exhibits exceptional photocatalytic activity: achieves almost total decolorization of MB dye in 60 min of irradiation. The table discussed above represents the degradation curve of MB dye over a temporal scale by Cu@ZnO as a photocatalyst. Cu@ZnO photocatalyst has shown excellent photocatalytic activity for the degradation of MB dye under sunlight. The results from this investigation highlight the promise of Cu@ZnO as an efficient and environmentally friendly photocatalyst for water treatment applications.

5 Conclusion

- In this work, we synthesized a highly efficient Cu@ZnO nanomaterials photocatalyst using a sustainable and eco-friendly hydrothermal method. Hibiscus rosa-sinensis leaf extract acted as a reducing and capping agent during synthesis.
- The synthesized material was characterized using XRD, FTIR, UV–Vis, FE-SEM–EDX, and HR-TEM-SAED techniques.
- Photocatalytic studies illustrated the efficient removal of MB dye under UV–visible light irradiation, with the degradation reaching as high as 97.67% within 60 min.
- Kinetics analysis showed that the photodegradation process had followed first-order kinetics, with a rate constant (k) of 0.03390 min^{-1} and a half-life ($t_{1/2}$) of 20.44 min.
- Other reasons for photocatalytic activities include Unique structural properties that result in efficient charge separation and transfer. Generation of reactive oxygen species (ROS) under light irradiation. Synergistic effect of copper doping. Increased surface area of ZnO nanomaterials.
- This work demonstrates the potential for developing effective and eco-friendly photocatalysts to remove water-soluble organic dyes from wastewater.

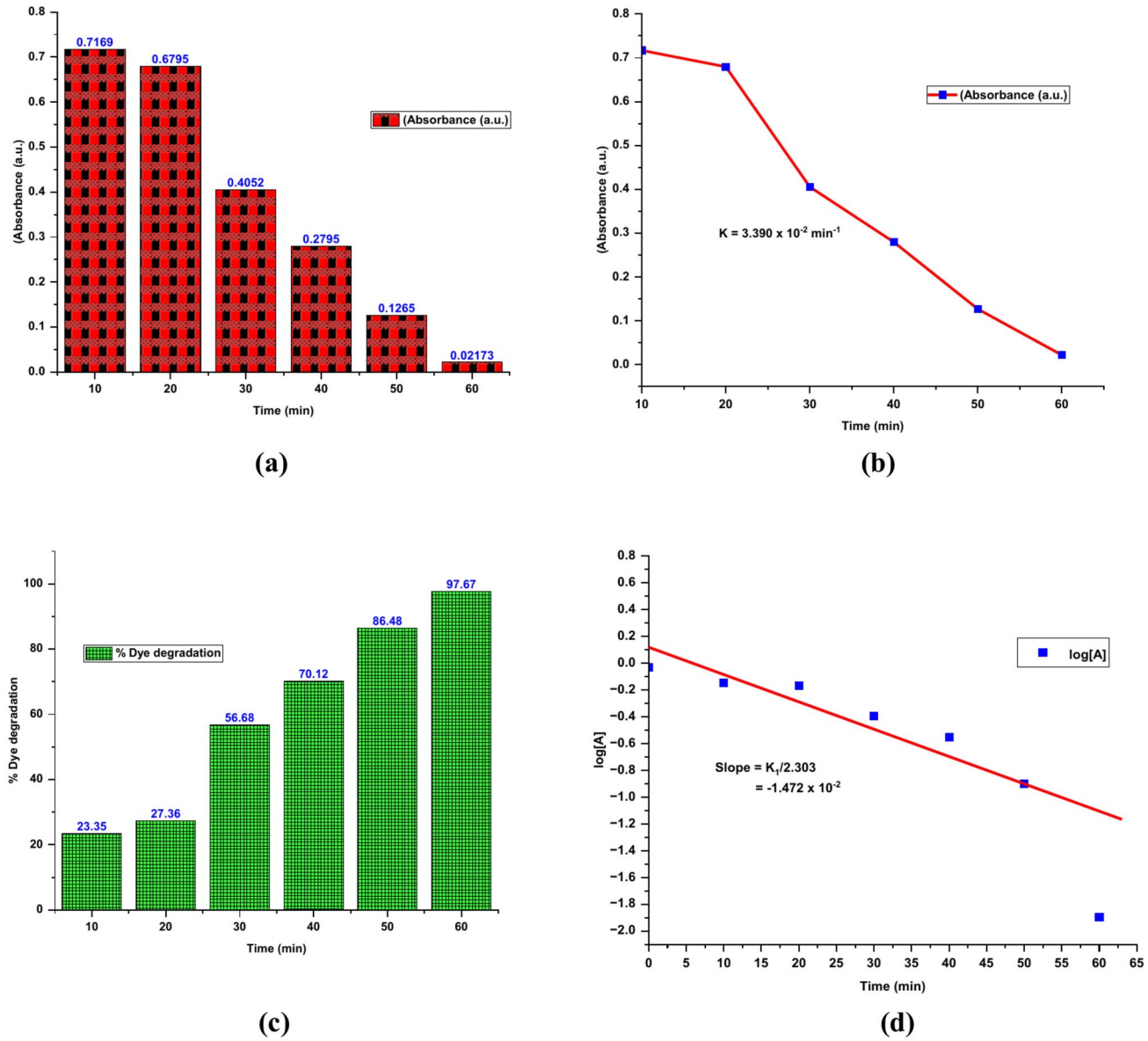

Fig. 15 Graphs of **a** and **b** Absorbance vs time (min), **c** and **d** % MB dye degradation vs time (min)

Author Contributions Vikram Jadhav: Writing—Original Draft, investigation, methodology. Umesh Dheple: Supervision, Resources, Validation, Pradnya Raut: Conceptualization, Data Curation, Writing—Original Draft. Seema Nikam: Editing, Investigation, Formal Analysis, Arun Bhagare: Writing—Review & Editing.

Data Availability No data was used for the research described in the article.

Declarations

Competing Interests The authors declare that they have no known competing financial interests.

References

1. Arfin T, Bhaisare DA, Waghmare SS (2021) Development of a PANI/Fe(NO 3) 2 nanomaterial for reactive orange 16 (RO16) dye removal. Anal Methods 13(44):5309–5327. https://doi.org/10.1039/D1AY01402A
2. Ismail M et al (2019) Pollution, toxicity and carcinogenicity of organic dyes and their catalytic bio-remediation. Curr Pharm Des 25(34):3645–3663. https://doi.org/10.2174/1381612825666191021142026
3. Mohammad F, Arfin T, Al-lohedan HA (2019) Enhanced biosorption and electrochemical performance of sugarcane bagasse derived a polylactic acid-graphene oxide-CeO2 composite. Mater Chem Phys 229:117–123. https://doi.org/10.1016/j.matchemphys.2019.02.085
4. Ahmad S, Singh R, Arfin T, Neeti K (2022) Fluoride contamination, consequences and removal techniques in water: a review. Environ Sci 1(5):620–661. https://doi.org/10.1039/D1VA00039J

5. Oladoye PO, Ajiboye TO, Omotola EO, Oyewola OJ (2022) Methylene blue dye: toxicity and potential elimination technology from wastewater. Results Eng 16:100678. https://doi.org/10.1016/j.rineng.2022.100678
6. Baste Y et al (2023) Polyol synthesis of Ag-doped copper oxide nanoparticles as a methylene blue-degrading agent. Catalysts 13(7):1143. https://doi.org/10.3390/catal13071143
7. Sajjadi SM, Hossinzadeh G (2024) Textile dyes removing from the wastewater by green synthesized Cu-doped ZnO photocatalysts under the simulated sunlight illumination. Ceram Int 50(19):36271–36285. https://doi.org/10.1016/j.ceramint.2024.07.011
8. Jadhav V et al (2024) Current advancements in functional nanomaterials for drug delivery systems. Nano-Struct Nano-Objects 38:101177. https://doi.org/10.1016/j.nanoso.2024.101177
9. Jadhav V, Roy A, Kaur K, Rai AK, Rustagi S (2024) Recent advances in nanomaterial-based drug delivery systems. Nano-Struct Nano-Objects 37:101103. https://doi.org/10.1016/j.nanoso.2024.101103
10. Raju P, Deivatamil D, Martinmark JA, Jesuraj JP (2022) Antibacterial and catalytic activity of Cu doped ZnO nanoparticles: structural, optical, and morphological study. J Iranian Chem Soci 19(3):861–872. https://doi.org/10.1007/s13738-021-02352-3
11. Dejam L et al (2023) ZnO, Cu-doped ZnO, Al-doped ZnO and Cu-Al doped ZnO thin films: advanced micro-morphology, crystalline structures and optical properties. Results Phys 44:106209. https://doi.org/10.1016/j.rinp.2023.106209
12. Khan SA, Noreen F, Kanwal S, Iqbal A, Hussain G (2018) Green synthesis of ZnO and Cu-doped ZnO nanoparticles from leaf extracts of *Abutilon indicum*, *Clerodendrum infortunatum*, *Clerodendrum inerme* and investigation of their biological and photocatalytic activities. Mater Sci Eng, C 82:46–59. https://doi.org/10.1016/j.msec.2017.08.071
13. Mohan R, Krishnamoorthy K, Kim S-J (2012) Enhanced photocatalytic activity of Cu-doped ZnO nanorods. Solid State Commun 152(5):375–380. https://doi.org/10.1016/j.ssc.2011.12.008
14. Singhal S, Kaur J, Namgyal T, Sharma R (2012) Cu-doped ZnO nanoparticles: synthesis, structural and electrical properties. Physica B Condens Matter 407(8):1223–1226. https://doi.org/10.1016/j.physb.2012.01.103
15. Onwudiwe DC, Arfin T, Strydom CA (2015) Surfactant mediated synthesis of ZnO nanospheres at elevated temperature, and their dielectric properties. Superlattices Microstruct 81:215–225. https://doi.org/10.1016/j.spmi.2015.02.003
16. Arfin T, Rangari SN (2018) Graphene oxide–ZnO nanocomposite modified electrode for the detection of phenol. Anal Methods 10(3):347–358. https://doi.org/10.1039/C7AY02650A
17. Obulapuram PK et al (2021) Adsorption, equilibrium isotherm, and thermodynamic studies towards the removal of reactive orange 16 dye using Cu(I)-polyaninile composite. Polymers (Basel) 13(20):3490. https://doi.org/10.3390/polym13203490
18. Arfin T, Rafiuddin (2012) Metal ion transport through a polystyrene-based cobalt arsenate membrane: application of irreversible thermodynamics and theory of absolute reaction rates. Desalination 284:100–105. https://doi.org/10.1016/j.desal.2011.08.042
19. Carmalinsophia A, Arfin T, Lima EC (2019) Recent developments in adsorption of dyes using graphene based nanomaterials. A new generation material graphene applications in water technology. Springer International Publishing, Cham, pp 439–471. https://doi.org/10.1007/978-3-319-75484-0_18
20. Onwudiwe DC, Arfin T, Strydom CA, Kriek RJ (2013) A study of the thermal and AC impedance properties of N-phenyldithiocarbamate complexes of Zn(II). Electrochim Acta 109:809–817. https://doi.org/10.1016/j.electacta.2013.07.176
21. Bushra R et al (2016) Development of PANI/MWCNTs decorated with cobalt oxide nanoparticles towards multiple electrochemical, photocatalytic and biomedical application sites. New J Chem 40(11):9448–9459. https://doi.org/10.1039/C6NJ02054B
22. Jadhav VR, Aher JS, Bhagare AM, Dhaygude AC, Lokhande DD (2022) Plant-mediated green synthesis of nanoparticles for photocatalytic dye degradation. Phytonanotechnology. Springer Nature Singapore, Singapore, pp 31–57. https://doi.org/10.1007/978-981-19-4811-4_2
23. Lu Y-H et al (2014) A facile green antisolvent approach to Cu^{2+}-doped ZnO nanocrystals with visible-light-responsive photoactivities. Nanoscale 6(15):8796. https://doi.org/10.1039/C4NR01607F
24. T. M. Jasiem, N. M. Nasser, S. K. Baderden, and H. A. Hasan, "Pharmacognostical and phytochemical studies of Iraqi Hibiscus rosa-sinensis," 2019, p. 040002. https://doi.org/10.1063/1.5123103.
25. Anand A, Sarkar B (2017) Phytochemical screening and antioxidant property of anthocyanins extracts from *Hibiscus rosa*-sinensis. Applications of biotechnology for sustainable development. Springer Singapore, Singapore, pp 139–147. https://doi.org/10.1007/978-981-10-5538-6_17
26. Garg D, Shaikh A, Muley A, Marar T (2012) In-vitro antioxidant activity and phytochemical analysis in extracts of Hibiscus rosa-sinensis stem and leaves. Free Radicals Antioxidants 2(3):41–46. https://doi.org/10.5530/ax.2012.3.6
27. Liu H et al (2010) The structure and magnetic properties of Cu-doped ZnO prepared by sol–gel method. Appl Surf Sci 256(13):4162–4165. https://doi.org/10.1016/j.apsusc.2010.01.118
28. Ashwini A, Saravanan L, Sabari V, Astalakshmi M, Kanagathara N (2023) Effect of Cu doping with varying pH on photocatalytic activity of ZnO nanoparticles for the removal of organic pollutants. Inorg Chem Commun 155:111137. https://doi.org/10.1016/j.inoche.2023.111137
29. Ferhat M, Zaoui A, Ahuja R (2009) Magnetism and band gap narrowing in Cu-doped ZnO. Appl Phys Lett. https://doi.org/10.1063/1.3112603
30. Soni SA, Jadhav VR, Kere TA (2018) Effect of copper substitution, calcination temperature, and photo-sensitizers on photocatalytic activity of Cu0.05 Zn0.95O. J Chem Environ Sci Appl 5(1):1–9. https://doi.org/10.15415/jce.2018.51001
31. Singh A, Wan F, Yadav K, Salvi A, Thakur P, Thakur A (2023) Synergistic effect of ZnO nanoparticles with Cu2+ doping on antibacterial and photocatalytic activity. Inorg Chem Commun 157:111425. https://doi.org/10.1016/j.inoche.2023.111425
32. Morales-Mendoza JE, Herrera-Pérez G, Fuentes-Cobas L, Hermida-Montero LA, Pariona N, Paraguay-Delgado F (2023) Synthesis, structural and optical properties of Cu doped ZnO and CuO–ZnO composite nanoparticles. Nano-Struct Nano-Objects 34:100967. https://doi.org/10.1016/j.nanoso.2023.100967
33. Kabbara H, Ghanbaja J, Noël C, Belmonte T (2017) Synthesis of Cu@ZnO core–shell nanoparticles by spark discharges in liquid nitrogen. Nano-Struct Nano-Objects 10:22–29. https://doi.org/10.1016/j.nanoso.2017.03.002
34. Karthik KV et al (2022) Green synthesis of Cu-doped ZnO nanoparticles and its application for the photocatalytic degradation of hazardous organic pollutants. Chemosphere 287:132081. https://doi.org/10.1016/j.chemosphere.2021.132081
35. Handago DT, Zereffa EA, Gonfa BA (2019) Effects of *Azadirachta indica* leaf extract, capping agents, on the synthesis of Pure And Cu doped ZnO-nanoparticles: a green approach and microbial activity. Open Chem 17(1):246–253. https://doi.org/10.1515/chem-2019-0018
36. Arunpandian M et al (2021) Fabrication of Cu/ZnO system: a dual performer as photocatalyst and luminescent material. Inorg Chem Commun 134:109022. https://doi.org/10.1016/j.inoche.2021.109022

37. Kadam AN, Kim TG, Shin DS, Garadkar KM, Park J (2017) Morphological evolution of Cu doped ZnO for enhancement of photocatalytic activity. J Alloys Compd 710:102–113. https://doi.org/10.1016/j.jallcom.2017.03.150
38. Labhane PK, Huse VR, Patle LB, Chaudhari AL, Sonawane GH (2015) Synthesis of Cu Doped ZnO nanoparticles: crystallographic, optical, FTIR, morphological and photocatalytic study. J Mater Sci Chem Eng 03(07):39–51. https://doi.org/10.4236/msce.2015.37005
39. Mariappan A, Pandi P, Beula Rani KR, Rajeswarapalanichamy, Neyvasagam K (2022) Study of the photocatalytic and antibacterial effect of Zn and Cu doped hydroxyapatite. Inorg Chem Commun 136:109128. https://doi.org/10.1016/j.inoche.2021.109128
40. Zafar MN, Dar Q, Nawaz F, Zafar MN, Iqbal M, Nazar MF (2019) Effective adsorptive removal of azo dyes over spherical ZnO nanoparticles. J Market Res 8(1):713–725. https://doi.org/10.1016/j.jmrt.2018.06.002
41. Silva H, Mateos-Pedrero C, Magén C, Pacheco Tanaka DA, Mendes A (2014) Simple hydrothermal synthesis method for tailoring the physicochemical properties of ZnO: morphology, surface area and polarity. RSC Adv 4(59):31166. https://doi.org/10.1039/C4RA05002A
42. Saxena G, Salmani IA, Mohd Khan S, Mohd Khan S (2023) Structural co-related optical properties of Al and Cu co-doped ZnO nanoparticles. Nano-Struct Nano-Objects 35:100986. https://doi.org/10.1016/j.nanoso.2023.100986
43. Pashchanka M et al (2011) A molecular approach to Cu doped ZnO nanorods with tunable dopant content. Dalton Trans 40(16):4307. https://doi.org/10.1039/c0dt01567a
44. Sabbaghan M, Nadafan M, Lamei HR (2021) Cu-doped ZnO synthesis by ionothermal method: morphology and optical properties. Opt Mater (Amst) 111:110679. https://doi.org/10.1016/j.optmat.2020.110679
45. Chithra MJ, Pushpanathan K (2016) Thermal, structural and optical investigation of Cu-doped ZnO nanoparticles. Mod Phys Lett B 30(34):1650406. https://doi.org/10.1142/S0217984916504066
46. Rooydell R, Brahma S, Wang R-C, Modaberi MR, Ebrahimzadeh F, Liu C-P (2017) Cu doped ZnO nanorods with controllable Cu content by using single metal organic precursors and their photocatalytic and luminescence properties. J Alloys Compd 691:936–945. https://doi.org/10.1016/j.jallcom.2016.08.324
47. Zhang Z et al (2008) Cu-doped ZnO nanoneedles and nanonails: morphological evolution and physical properties. J Phys Chem C 112(26):9579–9585. https://doi.org/10.1021/jp710837h
48. Mandavgane SA et al (2023) Kinetics and thermodynamic studies of photocatalytic hydrogen generation by Au/Pt/TiO2. Rasayan J Chem 16(04):2239–2248. https://doi.org/10.31788/RJC.2023.1648617
49. Obulapuram PK et al (2021) Surface-enhanced biocompatibility and adsorption capacity of a zirconium phosphate-coated polyaniline composite. ACS Omega 6(49):33614–33626. https://doi.org/10.1021/acsomega.1c04490
50. Kotkar SN, Gadekar GP, Singh RP, Rewatkar SB (2023) Solar light-driven photocatalytic decontamination of MB using Co and Cu doped ZnO with excellent antibacterial activity. Inorg Chem Commun 156:111197. https://doi.org/10.1016/j.inoche.2023.111197